Friction, acoustic emission, and wear mechanisms of a PEKK polymer

Malik Yahiaoui, France Chabert, Jean-Yves Paris, Valérie Nassiet, Jean Denape

Friction, acoustic emission, and wear mechanisms of a PEKK polymer

M. Yahiaoui*, F. Chabert, J-Y. Paris, V. Nassiet, J. Denape

Université de Toulouse, Laboratoire Génie de Production, France

Abstract

The tribological behavior of a steel/PEKK ball-on-flat contact was studied regarding the load, the velocity and the sliding distance in reciprocating or unidirectional motion. The friction measurements were synchronized with an acoustic emission (AE) device. The results show a behavior change associated with an adiabatic effect on the polymer when the mechanical energy input increases. Two interfacial mechanisms are also characterized: Schallamarch ridges and longitudinal ploughings. These mechanisms are related to two AE frequencies of 0.2 MHz and 1 MHz. The discussion on these two AE populations brings a stronger analysis and completes the friction and the wear mechanisms results.

Keywords: Polymers; Sliding wear; Thermal effects; Acoustic emission

1. Introduction

Among high performance polymers, thermoplastic polymers of PAEK family is one of the most resistant to work in severe conditions. The PAEK polymers display high thermomechanical and chemical resistance in many applications (e.g. seals, wire coating and compressor rings). For instance, the car industry is the first market share for the PAEKs, in particular because of their relatively low friction and high wear resistance [1].

Friction of polymers is generally described as the combination of adhesive forces on the surfaces and plastic deformation forces in the materials in sliding contact [2]. Therefore, adhesion (stick and slip) and hysteresis components are often observed during friction of polymers. In particular, concerning rubber-like materials, it was shown that the friction coefficient greatly increases towards the low loads [3]. This observation is explained in the Johnson-Kendall-Roberts (JKR) theory by the predominance of molecular attraction forces in lightly loaded contacts [4]. In addition, the friction of polymers, and especially elastomers, depends on the energy dissipation by viscoelastic loss which is sensible to the temperature and the sliding velocity.

As a results of these friction mechanisms, a pattern of ridges perpendicular to the sliding direction (i.e. Schallamach ridges) can appear on the worn surfaces as described by Schallamach concerning elastomers [5].

*Corresponding author.
Adress: Ecole Nationale d'Ingénieurs de Tarbes,
47 avenue d'Azereix 65016 Tarbes, France.
Tel.: +33 5624 42700; Fax: +33 5624 42708.
E-mail addresses: malik.yahiaoui@enit.fr

Several studies exposed the formation and propagation of Schallamach ridges in rubber-like polymers [6] and in thermoplastics with high thermomechanical properties (e.g thermoplastic polyurethane [7]).

Three main wear mechanisms commonly identified in polymers tribology are the adhesive wear, the abrasive wear and the fatigue wear [8]. In the literature, these mechanisms are presented by considering the direct interactions of the two materials in contact or by considering a tribofilm at the interface. Junctions between asperities and shearing mechanisms are related to adhesion. The ploughing of soft surface by hard asperities illustrates the abrasion. Propagation of cracks after cycles of periodical sliding friction is related to fatigue. Eventually, the interaction of wear particles at the interface and transfers on materials surfaces completes these analyzes with a third body approach [9].

Few papers expose the tribological behavior of polyetherketoneketone (PEKK) polymers. Most of the studies relate experiments and results concerning the wear behavior of polyetheretherketone (PEEK) and PEEK composite including ceramic particles. For example, Lu and Friedrich [10] showed that PEEK polymers with a high molecular weight have a better wear resistance. In a mechanical point of view, they found that the sliding velocity has a stronger influence than the load on the PEEK wear behavior. However, these authors added that pressure and velocity have a poor influence on friction of PEEK.

During friction and wear of materials, acoustic emission (AE) is generated in the contact. AE defines transient mechanical waves produced by the release of elastic stress energy from a localized source. Baranov et al. [11] identified different sources of AE (e.g. cracks propagation and debris formation) and their associated range of energy and of frequency in the sliding contacts. They also specified a list of material physicochemical and mechanical properties and friction conditions affecting AE amplitude. For example, a rough relief, a high hardness and an abrasive wear are factors of increase in AE amplitude. Conversely, fine grains, slow sliding velocity and adhesive wear are factors of decreasing amplitude of the AE signals. Lately, Yahiaoui et al. [12] completed this analyse using a third body approach. The AE energy dissipated by the sliding contact is function of the localization of AE sources (e.g. in the bodies in contact, in the third body) associated with the nature and the accommodation modes of these sources (e.g. deformation, fracture, rolling particles). Hase et al. [13] performed a review on wear mechanisms and AE signals and built an interesting correlation map of AE frequency spectra. This map indicates that the AE frequency band generated by sliding friction (i.e. asperities adhesion and third body shearing) was mainly observed between 20 kHz and 300 kHz [14, 15, 16]. Abrasive wear (i.e. cutting, ploughing or fragmentation by relatively sharp asperities) was related to AE signals located between 200 kHz and 1 MHz [17]. Severe wear or adhesive wear (i.e. detachment and transfer of material consecutive to an adhesive interaction and plastic deformations) was related to AE signals at higher frequencies between 1 MHz and 1.5 MHz [18].

Few tribological studies were focused on PEKK polymers. More generally, the literature shows that there is a clear lack of correlations between AE signals and tribological mechanisms. In this way, the aim of this paper is to bring a new characterization of the main tribological mechanisms in a steel ball on flat PEKK polymer contact using AE signals. In this scope, this study is based on the analysis of friction, wear and the

AE hits, signal energy and signal frequency.

2. PEKK properties

2.1. Physicochemical properties

The high performance semicrystalline polyaryletherketone Kepstan-6002 (Arkema company) is made of etherketoneketone copolymer with an ether/ketone ratio of a half. This PEKK was chosen because of its stiffness over a wide range of temperature. After the manufacturing process, the injection molded specimens contain 0.35 % of water and its density is about $1268\,\mathrm{kg}\cdot\mathrm{m}^3$.

DSC scans were performed with a DSC-Q200 from TA starting at room temperature to 400 °C with a ramp of to 5 °C/min. Samples were studied as received, with keeping its thermomechanical history, to be as close as possible to industrial conditions. After cooling to room temperature at 5 °C/min, a second ramp at same ramp speed was recorded. The thermogram (Fig. 1) displays a glass transition at 160 °C, followed by a low intensity peak due to water release just after the glass transition, when the macromolecular chains have gained enough mobility to move slightly. Then, we observe a cold crystallization with a maximum at 250 °C followed by a melting temperature centered at 305 °C for the first ramp. The enthalpy of crystallization ($\triangle H_\mathrm{c} = 14.9\,\mathrm{J/g}$) is lower than the enthalpy of melting, ($\triangle H_\mathrm{m} = 33.7\,\mathrm{J/g}$) indicating that the specimens were slightly crystalline before testing, due to the injection molding process. The crystalline rate is usually given by the ratio $\triangle H_\mathrm{m}/\triangle H_{100\%}$, but it cannot be calculated since the $\triangle H_{100\%}$ is not known due to the novelty of this polymer. During the cooling ramp, no cold crystallization occurs. The glass transition is measured at 150 °C. During the second ramp, the enthalpy of crystallization is measured at 13.5 J/g, identical to the enthalpy of melting, indicating that all the crystalline structure forms during the ramp at 5 °C/min is melted. The kinetics of crystallization is slow for this grade compared to other PAEK, allowing thoroughly controlling the crystalline rate along the processing steps.

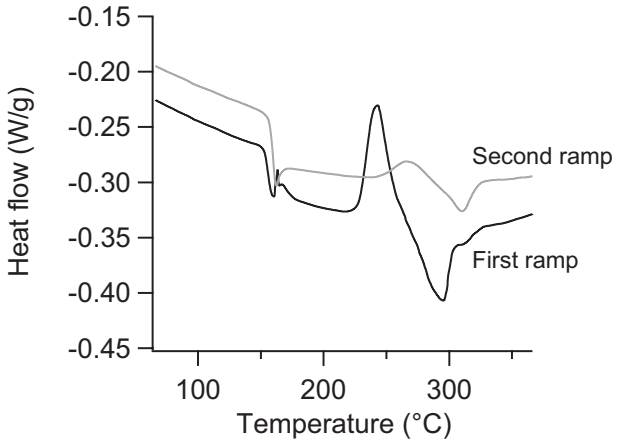

Figure 1: DSC curves of PEKK (endothermic peak downwards).

2.2. Thermomechanical characterization

The PEKK rheometrical behavior was obtained by using a rheometer ARES from Rheometric Scientific at 23 °C in oscillatory mode. The sample was set in torsional geometry. Temperature sweep at 3 °C/min to obtain elastic modulus (G') and viscous modulus (G") was performed at 1 % strain and 1 rad/s frequency within the viscoelastic linear domain. The G' and G" shear moduli over temperature are presented in Fig. 2 from room temperature to melting. The elastic modulus stays as high as 1 GPa up to 140 °C when the effect of glass transition begin to appear, resulting in the drop of elastic modulus of about 2 decades. In the same time, the loss modulus G" is 10 MPa at room temperature and increases to 100 MPa before reaching the glass transition. This increase is usually due to stress relaxation as polymeric chains gain more and more energy allowing them to change conformation to minimize their energy. After the glass transition, the specimen releases water as shown in the first peak and then it is subjected to cold crystallization from 220 to 250 °C, resulting in an increase of both elastic and viscous moduli. The value of 20 MPa for G' and 2 MPa for G" should be kept in mind for the values of plateaus after full crystallization of this grade.

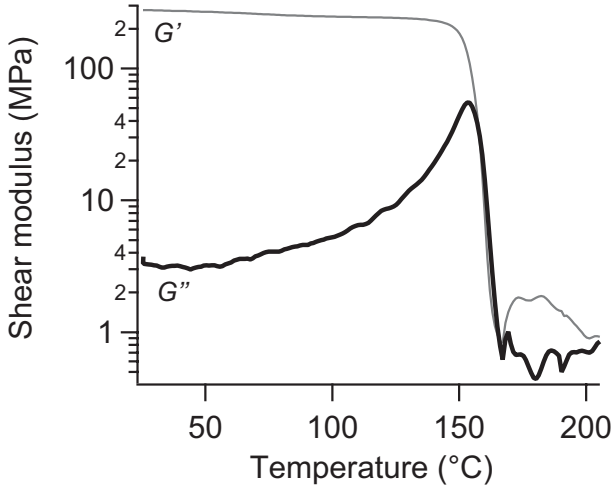

Figure 2: DMTA curves of PEKK with the storage modulus G' and the loss modulus G''.

The PEKK viscoelastic behavior was analyzed using a relaxation curve obtained at 1 % strain at 23 °C (Fig. 3). The curve displays a classical viscoelastic behavior with a torsional modulus exponentially decreasing during the relaxation. The complete relaxation is achieved after 4000 s. More accurately, the generalized Maxwell model was used to fit this relaxation curve. Three characteristic times were needed to fully describe the experimental curve: 8.4 ± 0.3 s, 201 ± 3 s and 1806 ± 31 s.

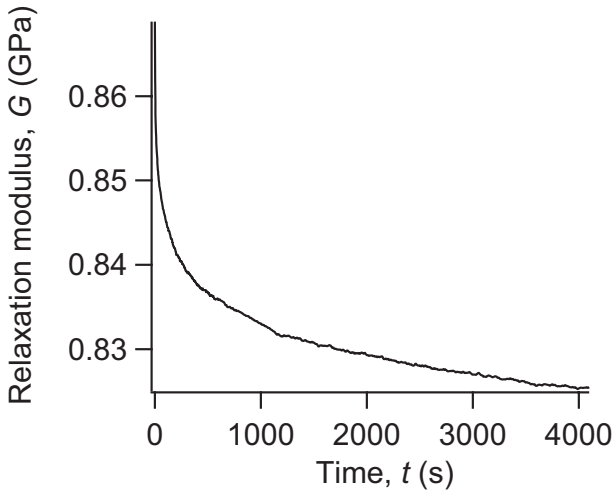

Figure 3: Stress relaxation test of PEKK.

3. Experimental device

3.1. Linear tribometer

A microscratch test device (CSM MST) was used as a linear tribometer (Fig. 4). This tribometer performed a sliding contact between a 100Cr6 steel ball with a diameter of 6 mm and a flat PEKK sample (52 mm × 10 mm × 3.3 mm). The experiments can be carried out in reciprocating or unidirectional motion with an unloading stage after each stroke.

Acoustic emission acquisitions were performed using a sensor fixed on the PEKK surface. This sensor (Pico sensor from Euro Physical Acoustic) is a large band type operating at its maximum sensitivity between 100 kHz and 1 MHz. The sensor was fixed on the PEKK surface at one extremity using a water-based adhesive containing styrene acrylic copolymer. This adhesive allows a good transmission of acoustic signals, dries in few seconds and the sensor is easily detached after the experiments. The coupling between the sensor and the PEKK sample was then controlled by the Hsu-Nielsen source method described by the standard NF EN 1330-9. Another acoustic emission sensor is integrated in the linear tribometer and fixed near the ball holder. This sensor gives a complementary information of amplitude of acoustic emission signals synchronized with mechanical data acquired by the device. In this study, no significant decay was observed on the AE signals during the tests performed at different positions on the sample surface.

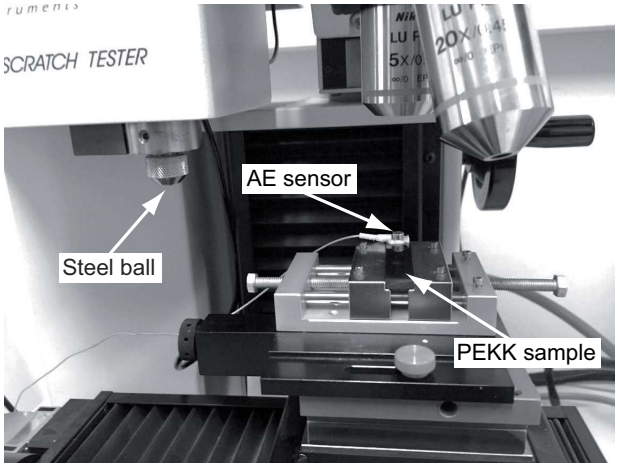

Figure 4: View of the linear tribometer and the experimental setup.

3.2. Experimental procedure

Three experimental campaigns were carried out to study the effects of load, velocity, number of strokes and the difference between reciprocating and unidirectional motion of the tribological behavior of the steel ball sliding against the PEKK:

- The first campaign considered the effect of load with a sliding velocity of 100 mm/min over a travel distance of 250 mm (i.e. 50 strokes of 5 mm) in reciprocating and unidirectional motion. Four constant normal loads were chosen at 1, 10, 20 and 30 N.
- The second campaign concerned the effect of velocity with a constant load of 30 N over a travel distance of 250 mm in reciprocating motion. Five sliding velocities were selected at 10, 50, 100, 300 and 500 mm/min.
- The third campaign was focuses on the effect of the number of strokes. Five different number of strokes were selected: 1, 2, 3, 4, 50 and 742 to study the early stage of wear and the long term wear on the PEKK surface. As one stroke represents a sliding distance of 5 mm, the overall travel distance varied from 5 mm to 3.71 m.

Before testing, the surface of the PEKK samples were polished leading to a surface roughness R_a of 65 ± 9 nm. The samples were not dried and were cleaned with ethanol. Each experiment was repeated twice. The average values and their associated errors were calculated from this repeatability. No wear was observed on the ball after the experiments.

3.3. Acoustic emission signals

During experiments, the acoustic emission signals i.e. hits (Fig. 5) were sampled considering the parameters defined in Table 1. Two signal characteristics were considered: the absolute acoustic energy and the centroid frequency. The absolute acoustic energy E_a is extracted by integrating the absolute value of the

acquired hits (Fig. 5a) over the sampling periods. The centroid frequency represents the frequency center of mass of the acoustic emission signals and it characterizes the overall frequency content of an acoustic emission signal (Fig. 5b). These parameters are used to follow any significant changes in the sliding contact behavior and to complete the mechanical information given by the friction coefficient.

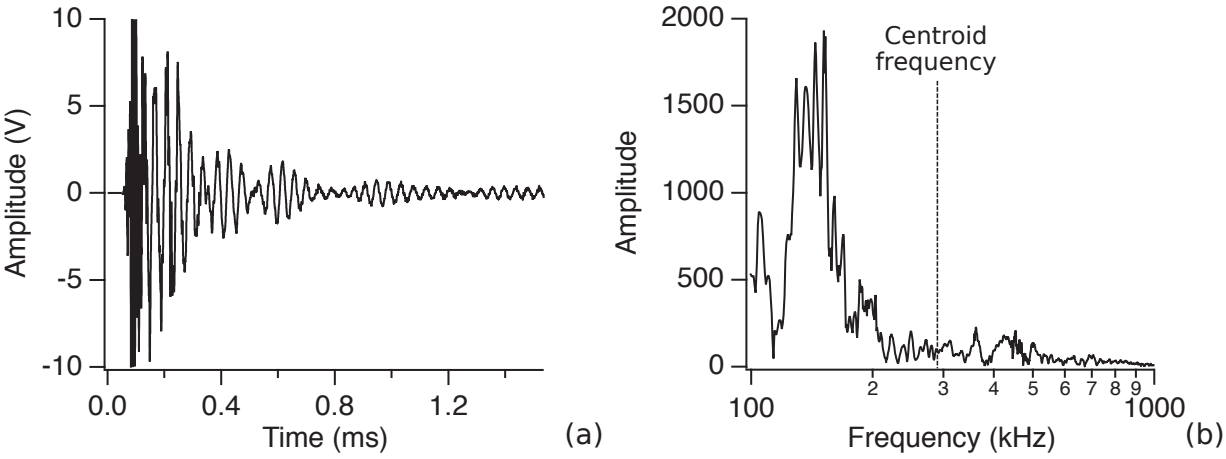

Figure 5: Acoustic emission raw signal: a - temporal hit wave; b - FFT of a hit.

Table 1: Acquisition parameters of acoustic emission signals with the peak definition time (PDT), the hit definition time (HDT) and the hit lockout time (HLT).

Threshold (dB)	Preamplification (dB)	Sample rate (MHz)	Pre-trigger (µs)	PDT (µs)	HDT (µs)	HLT (µs)
29	40	10	50	200	800	1000

4. Friction results

4.1. Effect of load

The friction μ coefficient displays an oscillating form around an average tendency $\langle\mu\rangle$ until the end of the experiments (Fig.6a). These oscillations seems to enter a permanent regime after a sliding distance of 50 mm. They are characterized by an alternance of high friction coefficient phase (HF) and low friction phase (LF). The nature of this hysteresis friction is related to the macroscopic viscoelastic deformations and the energy dissipated by molecular relaxation process in the polymer during sliding. As seen above with the PEKK, the first viscoelastic relaxation time is about ten seconds and it takes more than one hour for the polymer to be totally relaxed. During sliding friction, the polymer is in compression in front of the spherical indenter. And as described by Cherry [19], behind the indenter, the viscoelastic recovery will assist the forward motion of the indenter. This explains the HF and LF phases and implies that the first stroke influences the succeeding strokes during an experiment.

The amplitude of the hysteresis phenomenon tends to be reduced with the applied load. Actually, there is a distinct change of friction behavior between 10 N and 20 N. At low loads, the instantaneous friction

coefficient μ slightly increases during the HF phases. During the LF phases, μ slightly decreases. At higher loads, μ still increases during HF phases at the beginning of the test until an accommodation sliding distance (130 mm at 20 N and 50 mm at 30 N). Then, μ decreases and tends to reach the constant value observed during the LF phases. Here, μ also exhibits significant peaks of adhesion between each stroke. These variations of friction may indicate a rheology change of the surface and subsurface at high load due to an adiabatic heating effect.

More generally, the friction coefficient average $\bar{\mu}$ exponentially decreases with the load and reaches a constant value of 0.31 ± 0.01 at the high loads (Fig. 6b). This observation may be consistent with what was measured with rubber-like materials [20] and the JKR theory [4]. In this case, the increase of the friction coefficient towards the low loads should be related to the contribution of molecular attraction forces when the load application decreases.

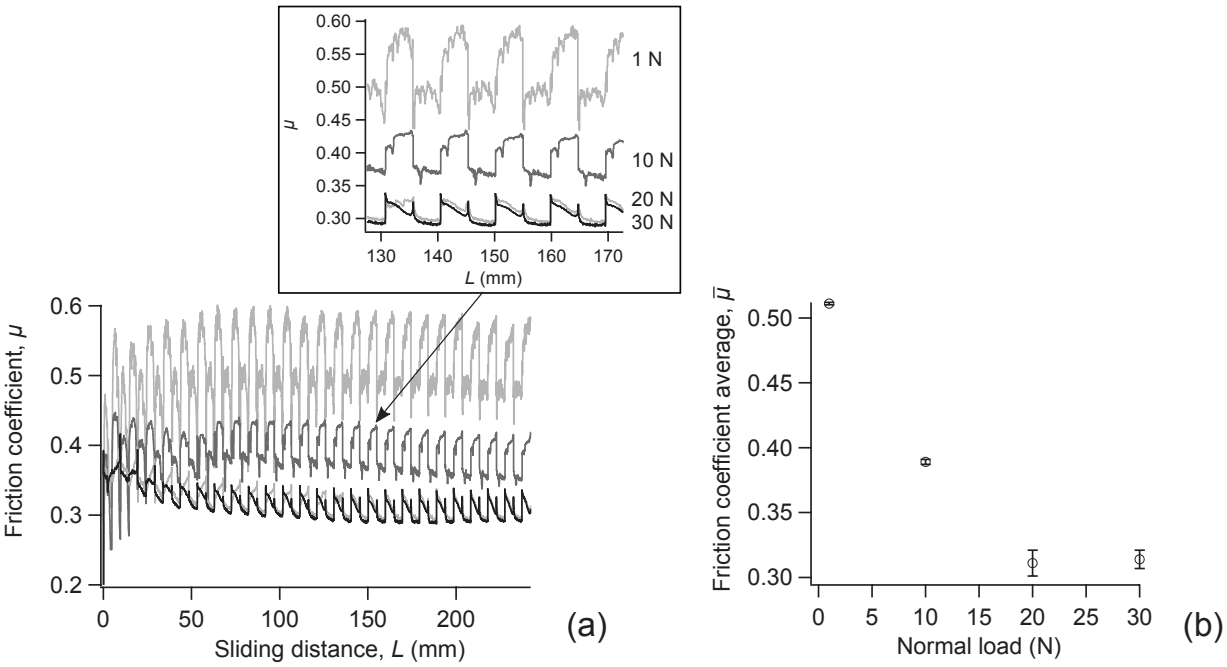

Figure 6: Effect of the applied load on friction in reciprocating sliding motion: a - friction coefficient vs. sliding distance; b - mean friction coefficient vs. load.

Concerning the acoustic emission, the hits were acquired on a centroid frequency range from 200 kHz to 1200 kHz. More precisely, two main peaks P1 and P2 can be respectively identified at frequencies of 247 ± 15 kHz and 1028 ± 27 kHz (Fig.7a). More hits are acquired around the P1 peak. The P1 peak is also by far the more energetic and it increases with the applied load (Fig.7b). P1 amplitude increases with the load and conversely, P2 amplitude decreases with the load.

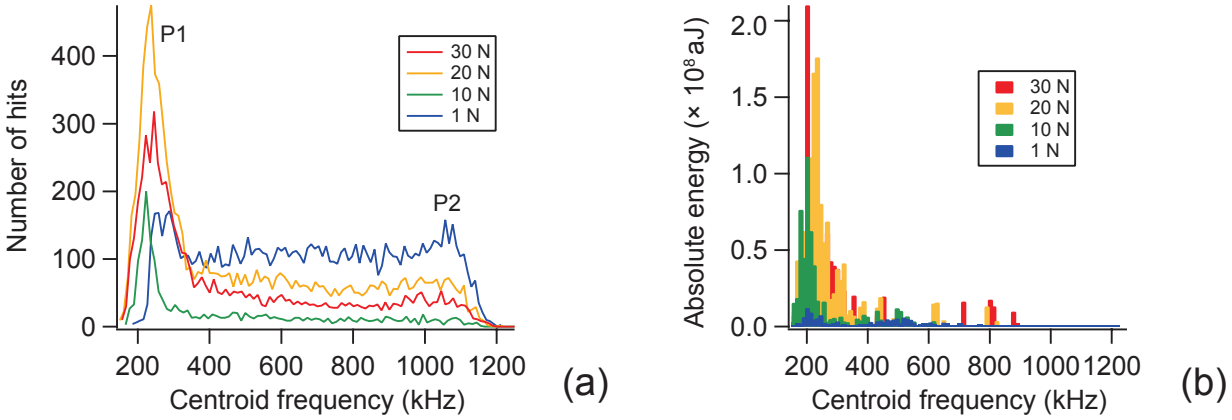

Figure 7: Centroid frequency spectrums regarding to the different loads in reciprocating motion: a - hits distribution; b - absolute energy distribution.

The acoustic emission signals display a higher amplitude during the LF phases (see the friction coefficient and AE amplitude superimposition (Fig. 8). At 1 N, the peaks of acoustic emission amplitude are only detected during the LF phases (Fig. 8a). At higher loads, they are clearly higher during the LF phases than the HF ones (Fig. 8b). These curves also display a drop of acoustic energy with the sliding distance. At 30 N, the acoustic emission amplitude decreases and is under the detection threshold after a sliding distance of 100 mm.

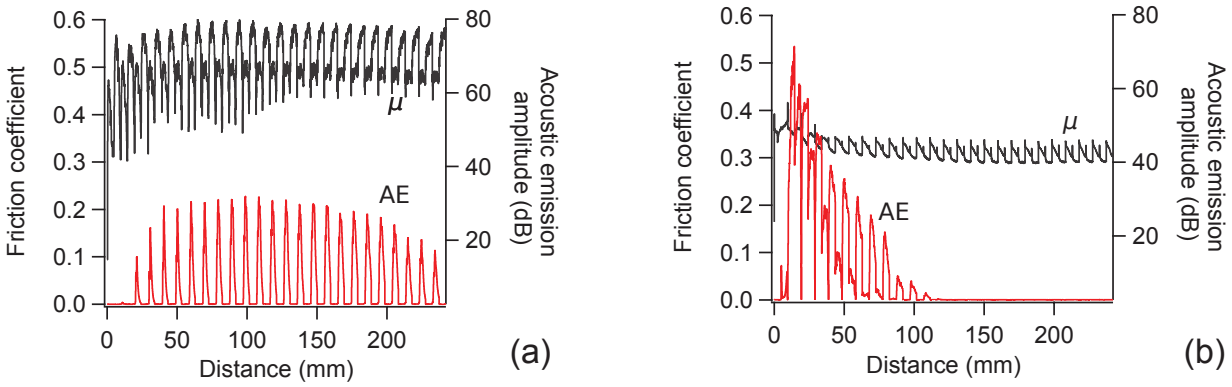

Figure 8: Amplitude of acoustic emission signals and friction coefficient curves: a - at 1 N; b - at 30 N.

4.2. Effect of velocity

The velocity has no effect on the friction coefficient μ general oscillating form (Fig. 9a). Nevertheless, μ decreases with the sliding velocity. The adhesion peak (stick period) between each strokes decreases with the velocity. The friction coefficient average $\bar{\mu}$ exponentially decreases with the sliding velocity (Fig.9b). In other words, the friction mainly decreases with the velocity but the friction evolution during sliding does not vary. That indicates that the main interface mechanisms during strokes should remain unchanged. For instance, a thermal effect induces by the increase of velocity affecting the polymer cohesive mechanisms could explain the change of friction amplitude. As exposed by Tabor in its review of friction of polymers

[21], for higher speeds, the effect of speed on friction is complicated to calculate because of the combination of heating and mechanical shear strain. The friction produces heating at the interface and in the subsurface. The temperature rise modifies the rheological properties of the polymer. In addition, a higher speed induces higher shear-strains and possibly modification in the polymer structure.

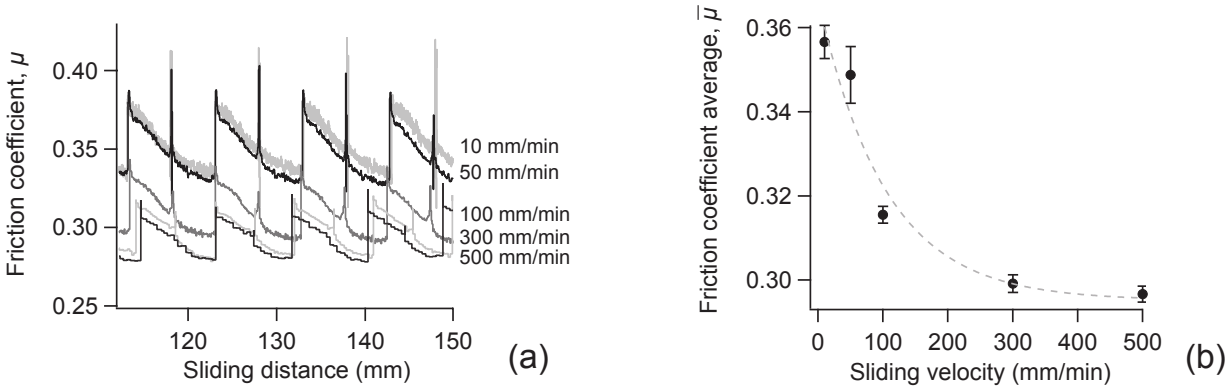

Figure 9: Effect of the sliding velocity on friction at a normal load of 30 N: a - friction coefficient vs. sliding distance; b - mean friction coefficient vs. load.

The acoustic emission events still occurring in greater proportion and with a higher energy around the P1 peak (Fig. 10a). The overall number of hits decreases after a sliding velocity of 50 mm/min. The AE amplitude decreases when the velocity is increased from 300 mm/min to 500 mm/min (Fig. 10b). Baranov et al. [11] present several factors decreasing AE amplitude as a light load, a slow sliding velocity, a smooth relief or an elevated contact temperature. As the load and surfaces in contact remain unchanged, this would confirm a contact heating effect on friction.

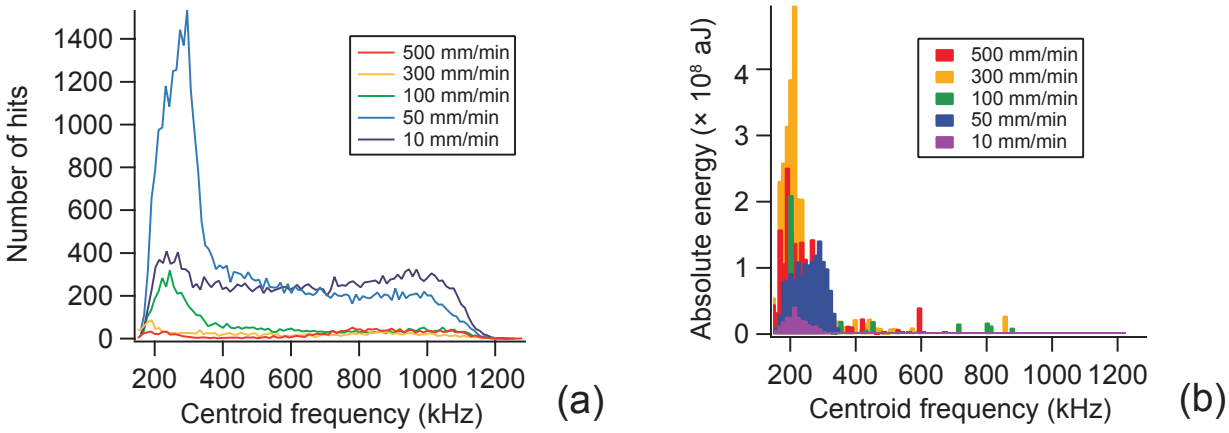

Figure 10: Centroid frequency spectrums regarding to the sliding velocities in reciprocating motion: a - hits distribution; b - absolute energy distribution.

4.3. Evolution with sliding distance

The nominal experiments are performed during 50 strokes (i.e. 250 mm) and during these tests, the average friction $\langle \mu \rangle$ seems to reach a steady state. However, after these 50 strokes, the contact continues to

evolve and $\langle\mu\rangle$ tends to reach another plateau after 200 strokes (i.e. 1000 mm) (Fig. 11). The instantaneous friction μ keeps the same form all along the long distance experiment.

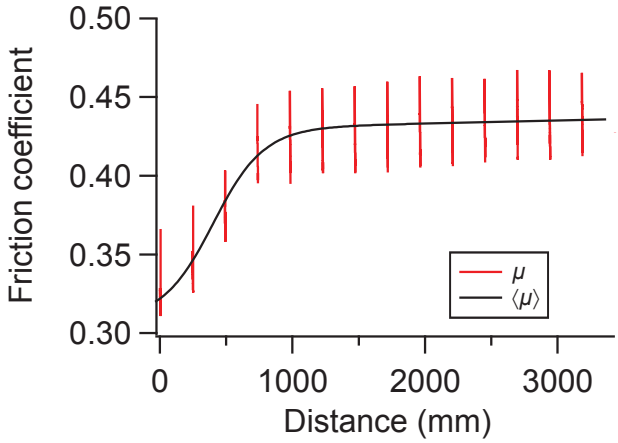

Figure 11: Effect of the sliding distance on friction at 30 N and 100 mm/min (here, the signal was only acquired every 50 strokes i.e. 250 mm).

At few strokes, the acoustic emission is only represented by the P1 peak (Fig. 12a). At tens of strokes, the different characteristic bands of frequencies are in the same order of hits and the associated contact mechanisms are then quite balanced. At long term, the P1 peak becomes preponderant. As seen above, at the end of the nominal number of strokes (i.e. 50), the number of hits drops and no events are detected (i.e. constant cumulated hits) until a little more than 400 strokes (i.e. 2000 mm) (Fig. 12b). Then new events are detected with a constant number of hits (i.e. linear cumulated hits). This AE break during the test clearly indicates a transition mechanism at the interface.

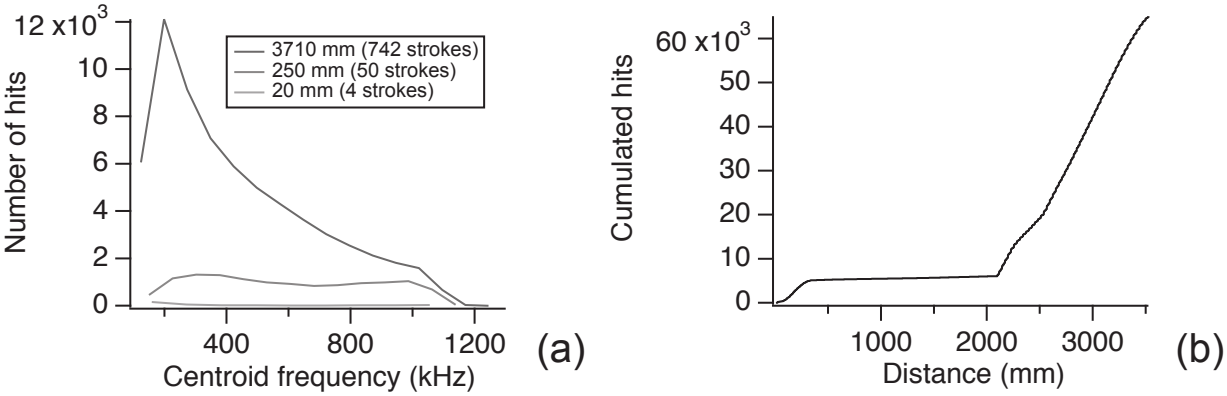

Figure 12: Acoustic emission analysis regarding to the sliding distance in reciprocating motion at 30 N and 100 mm/min: a - Centroid frequency spectrums; b - Cumulated hits.

4.4. Unidirectional friction

During experiment in unidirectional motion, the instantaneous friction coefficient μ is quite constant after transient conditions over a distance of 50 mm (Fig. 13). In unidirectional motion, as the viscoelastic recovery does not meet a forward motion of the indenter, μ does not display a hysteretic behavior. The average

friction coefficient $\bar{\mu}$ stills exponentially decrease with the load because of the molecular attraction forces contribution. The friction in unidirectional motion is at least 10 % lower than in reciprocation motion.

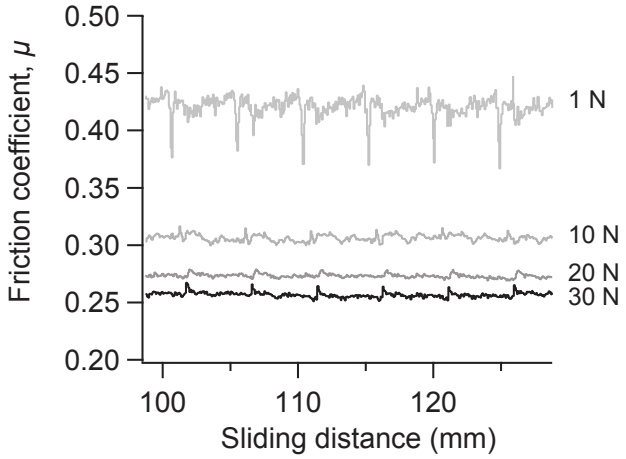

Figure 13: Effect of the applied load on friction coefficient in unidirectional sliding motion.

At low loads, the number of hits for the P2 peak is here greater than for the P1 peak (Fig. 14a). The P1 peak is not observed at 1 N. At higher loads, the P2 peak amplitude decreases and tends to be lower than the P1. The acoustic emission energy of the population P1 is still predominant and represents most of the AE energy calculated here (Fig. 14b). Except for the lowest load of 1 N, this energy decreases with the load.

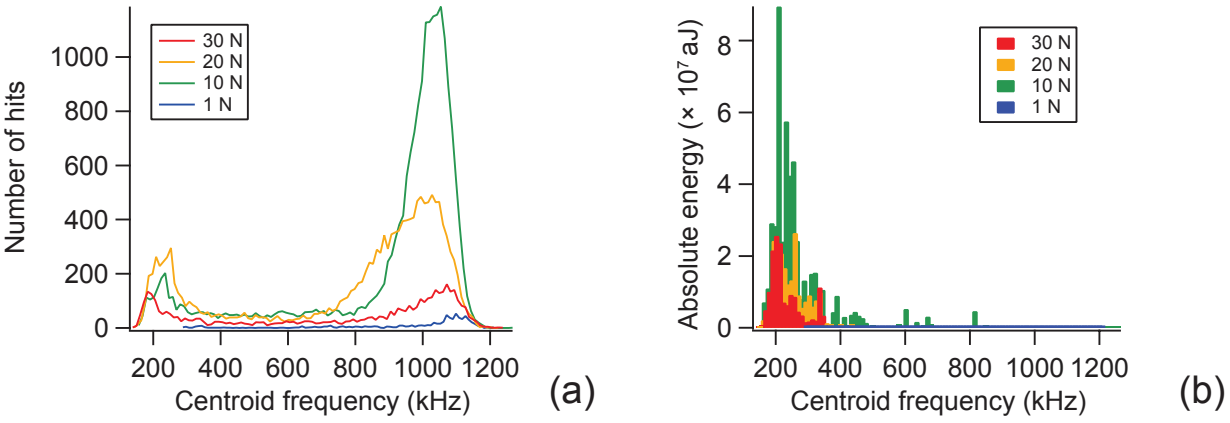

Figure 14: Centroid frequency spectrums in function of the load in unidirectional motion: a - hits distribution; b - absolute energy distribution.

5. Analyzes of wear tracks

5.1. Effect of load

As for the friction coefficient trend, the wear tracks display a similar aspect after a load of 20 N (Fig. 15). For instance, the wear track width is of 176 ± 8 µm at 1 N, 384 ± 16 µm at 10 N, 494 ± 39 µm at 20 N and 518 ± 16 µm at 30 N. At 1 N, the wear tracks show slight abrasion scratches and Schallamach ridges. Accumulated material and chips can also be observed at the extremities of the tracks. Few debris are present

on the wear tracks. At 10 N, Schallamach ridges and greater scratches are clearly visible on the tracks. At 20 N and 30 N, the surface of the wear tracks are covered by longitudinal ploughing. In addition, Schallamach ridges are observable on the edges of the tracks. These observations show that adhesive wear and ploughing are in competition here. When the load increases more longitudinal ploughing are formed and fewer ridges are visible.

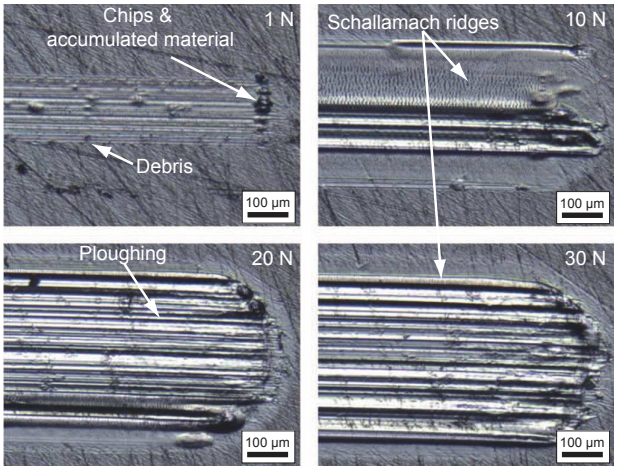

Figure 15: Optical microscope observations of a part of the wear tracks obtained after load experiments at 100 mm/min (the sliding direction is horizontal).

Optical topography measurements were performed using the Wyko NT1100 profilometer. This profilometry analysis also highlights a balanced association of ploughing and plastic deformation on the tracks. Plastic beads are formed at the extremities and the edges of the tracks counterbalancing the global deformation induced by the steel ball (Fig. 16a). These plastic beads are greater with a higher load. In addition, smaller plastic beads and ploughing microscratches are present inside the tracks (Fig. 16b).

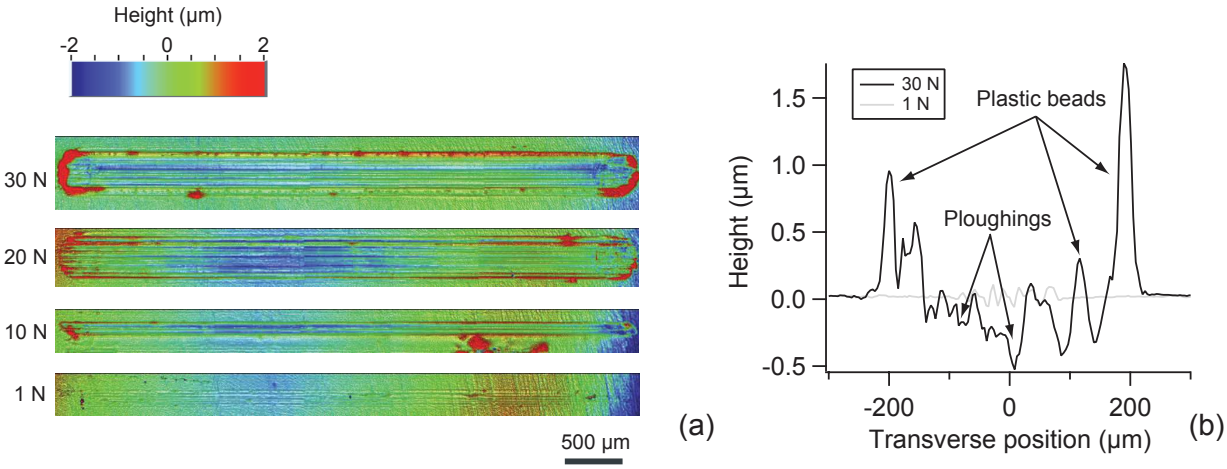

Figure 16: Optical profilometry analyzes after load experiments: a - topographies of the wear tracks; b - transverse profile of the tracks at 1 N and 30 N.

5.2. Effect of velocity

As for the asymptotic trend of the mean friction coefficient, the wear track aspect tends to stabilize after 100 mm/min (Fig. 17). The wear track width does not significantly change with the velocity with an averaged value of 495 ± 13 µm. At low velocity, Schallamach ridges cover more than a half of the worn surface. The rest is occupied by the longitudinal abrasion scratches. At the highest velocities, Schallamach ridges are only visible on the edges of the tracks and most of the surface shows longitudinal ploughings. Great plastic beads appears at the tracks extremities. At 500 mm/min, the wear track displays a smoother surface with finer scratches. These observations indicate a clear change of wear behavior. A thermomechanical effect on the polymer may account for this change by a variation of mechanical properties of the surface and the subsurface with an elevation of the contact temperature. This is a well-known mechanism usually defined as an adiabatic process due to non-conducting behavior of polymer and frictional heat causing thermal softening to interfacial layer only [22, 23].

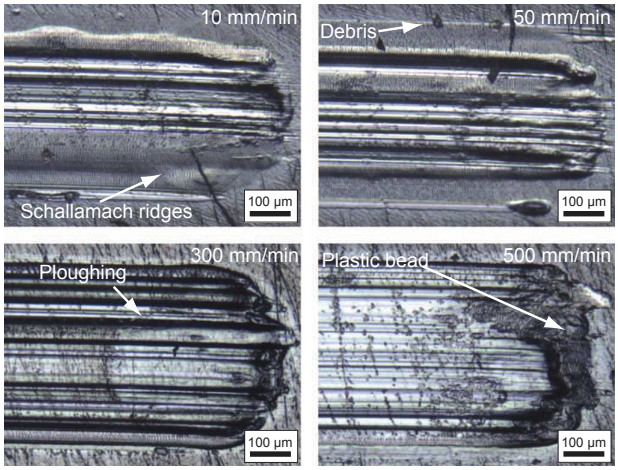

Figure 17: Optical microscope observations of a part of the wear tracks obtained after velocity experiments at 30 N (the sliding direction is horizontal).

5.3. Evolution with sliding distance

The observation of the wear tracks obtained after the experiments at 1 to 742 strokes shows the progressive formation of a plastic bead at the extremities (Fig. 18). Since the first strokes the abrasion mechanism forms scratches and debris. With the ridges displacement and rolls formation, more and more accumulated material is pushed towards the extremities of the wear track. At a longer term, when a critical volume of material is accumulated at these extremities, polymer is ejected from the contact by forming chips. The wear track after 742 strokes shows an evolution in the wear mechanisms of the interface. The wear track always displays scratches and ridges. However, the worn surface is smoother and seems thermally affected.

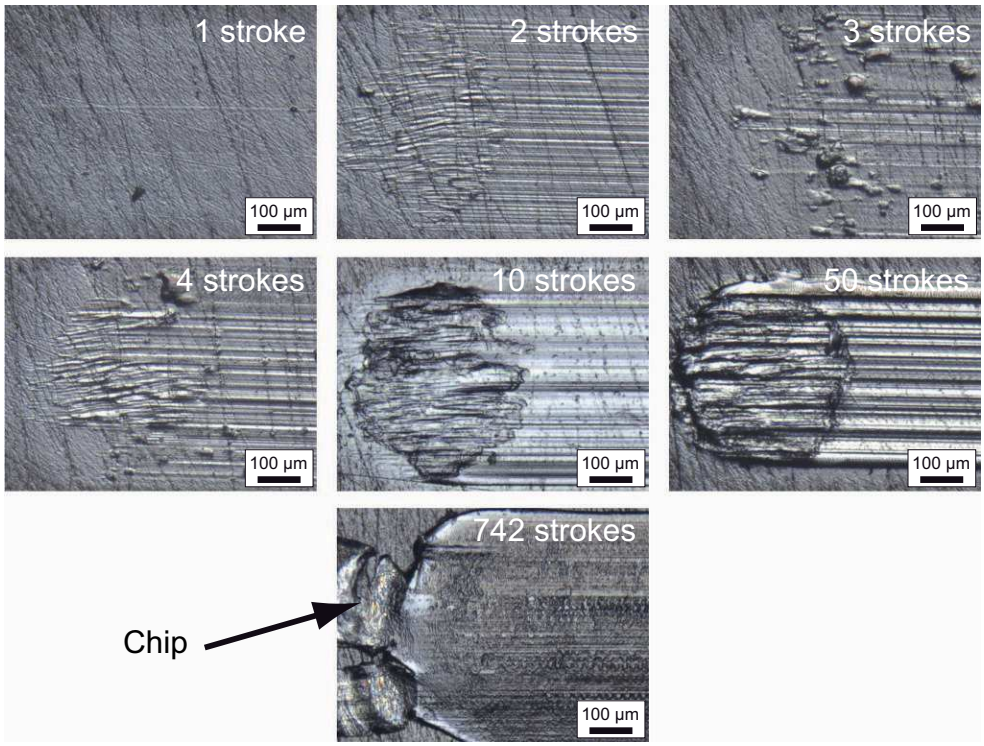

Figure 18: Optical microscope observations of a part of the wear tracks obtained with different number of strokes at 30 N (the sliding direction is horizontal).

At long sliding distance, the contact is dominated by more macroscopic plastic deformation. A continuous plastic bead surrounds the track (Fig. 19a) and, as confirmed by the profilometry analyzes, a clear conformity of the contact is formed (Fig. 19b). The volume of the bead corresponds to more than 79 % of displaced volume of material from the track.

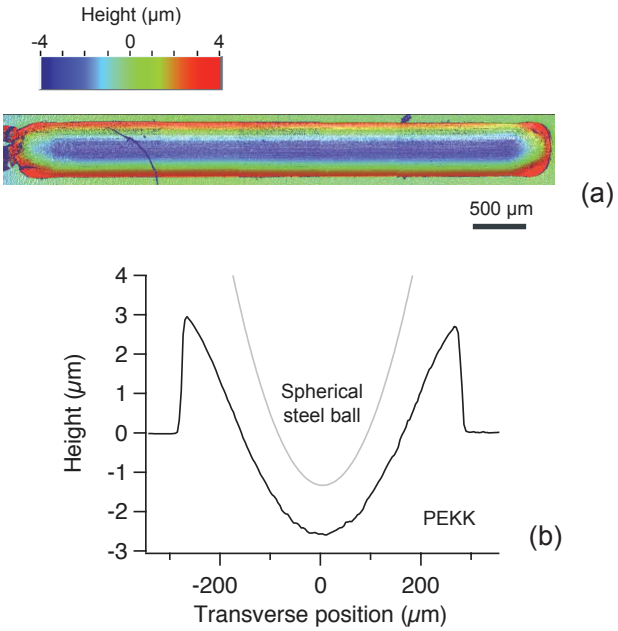

Figure 19: Optical profilometry analyzes after 742 strokes at 30 N: a - topographies of the wear track; b - transverse profile of the track.

5.4. Unidirectional friction

As above, wear tracks surface are a combination of longitudinal scratches, Schallamach ridges, accumulated material and detached particles (Fig. 20). However, as the tracks are resulting from repetitive unidirectional sliding friction, the polymer is pushed towards the sliding direction and material accumulates on one side of the tracks. This explains that no hysteresis effect is observed and that the friction remains constant in unidirectional friction. Indeed, when a certain conformity is reached between the two material pairs, the worn surface does not evolve before 50 strokes. At longer distance, the wear track should change because of the heating contribution described above.

Here, the Schallamach ridges have the aspect of stratified polymer layers as the result of successive material waves. Otherwise than in reciprocating motion, the Schallamach waves are here visible on all the track surface even at the highest load.

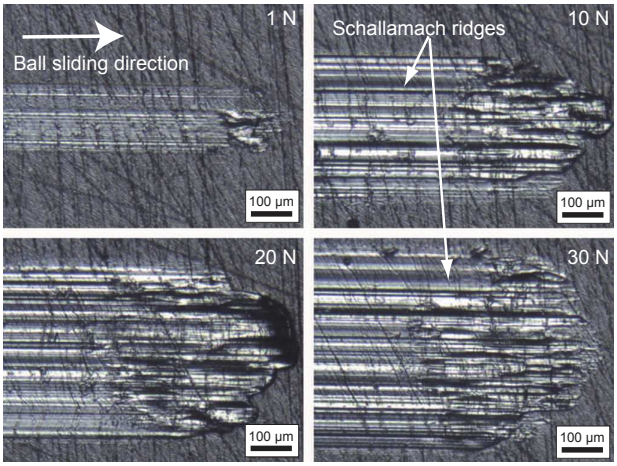

Figure 20: Optical microscope observations of a part of the wear tracks obtained after unidirectional sliding experiments (the sliding direction is horizontal and the ball slides on the flat from the left to the right).

6. Discussions

6.1. Adiabatic heating calculus

As discussed earlier, the PEKK can be subjected to an adiabatic heating effect on the surface and the subsurface leading to rheological change in the contact. A simple calculus can be made from this consideration using the following hypothesis:

- Most of the friction work during the overall sliding distance L is converted into heat Q in the contact (i.e. $Q = \mu \cdot F_{\mathrm{N}} \cdot L$) and a mass m of polymer (i.e. the adiabatic system with a specific heat $c = 1.28 \pm 0.15\,\mathrm{J \cdot g^{-1} \cdot K^{-1}}$ [24]) is warmed up.
- The change of rheological properties occurs above the glass transition corresponding to a temperature variation of ΔT of 130 K (i.e. the glass transition minus the room temperature).

The maximum mass of polymer heated can then be calculated using the classical thermodynamical equation $Q = m \cdot c \cdot \Delta T$. The maximum depth of PEKK heated can also be calculated from the observations of the wear tracks geometry. Obviously, the cumulated mechanical energy increases with the load and consequently the maximum mass heated and the maximum depth heated increase respectively from 0.7 to 13 µg and from 0.2 to 0.4 µm (Fig. 21a). These values of maximum depth heated are consistent with the plastic ploughings depth (see Fig. 16b). Regarding the previous results, a critical value of cumulated mechanical energy is between 1 and 1.5 J corresponding to a change of the PEKK rheology during the load experiments. This change corresponds here to an inflection of the maximum depth heated.

During the velocity experiments, the cumulated mechanical energy is always over 2.2 J (Fig. 21b). This explains that during the velocity experiments, the friction evolution is representative to what occurs during the load experiments after 10 N associated with a change of the polymer rheology. The maximum mass heated and the maximum depth heated decrease with the velocity respectively from 16 to 13.5 µg and from 0.4 to 0.6 µm.

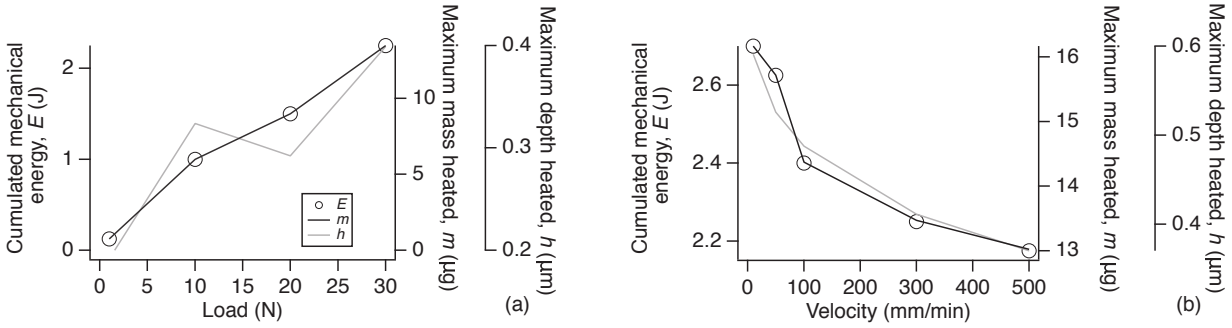

Figure 21: Cumulated mechanical energy, maximum mass heated and maximum depth heated: a - load effect; b - velocity effect.

6.2. Contact mechanisms & acoustic emission

The velocity accommodation is performed in the PEKK body and on the surface of the PEKK (Fig. 22). According to the cumulated mechanical energy E inputed in the contact, cohesive mechanisms occurs in the subsurface and interfacial mechanisms are here essentially visible on the surface of the PEKK. Under a cumulated mechanical energy of 2 J, most of the accommodation is performed by viscoelastic deformations followed by relaxations at the back of the contact. On the PEKK surface, longitudinal abrasion scratches are realized by sharp asperities of the steel counterface. Schallamach ridges are also formed by the adhesion of smooth counterface asperities on the polymer. Between 2 and 5 J, plastic deformations appears in the PEKK and adiabatic heating helps this mechanism. Longitudinal plastic ploughing are visible in the center of the contact where the PEKK is submitted to a higher contact pressure. On the side of the contact, where a lower contact pressure is distributed, Schallamarch ridges are formed. Above a cumulated mechanical energy of 5 J, a high conformity of the contact is reached and the contact won't greatly evolve. At the interface, slight viscoelastic and plastic deformations still occur. The PEKK worn surface as a relatively smooth aspect and ridges and ploughing mechanisms are a little visible.

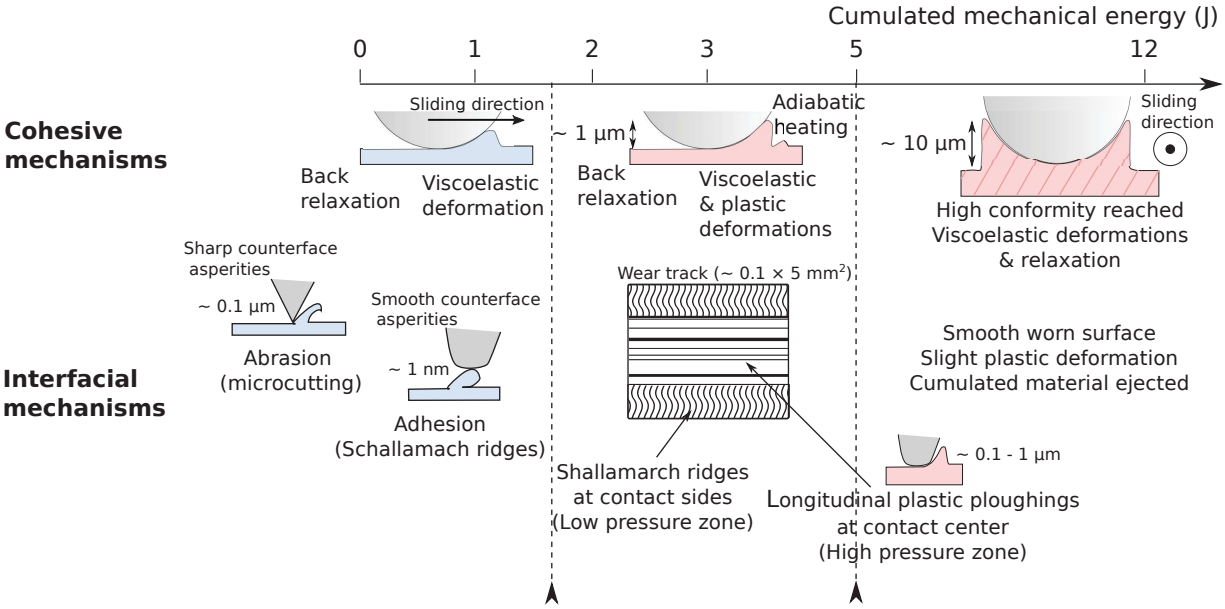

Figure 22: Cohesive and interfacial contact mechanisms as a function the cumulated mechanical energy.

Two main interfacial mechanisms are clearly discriminated by the acoustic emission frequency spectra: the asperities adhesion (nanometric size contacts) generating Schallamarch ridges and the asperities ploughing(micrometric size contacts) forming the longitudinal scratches. These two sources of acoustic emission were respectively associated with AE frequencies around 1 MHz and 0.2 MHz. The ridges formation by nanometric plastic deformation of polymer are less energetic than the larger longitudinal ploughings. When more and more cumulated mechanical energy is introduced in the contact, an adiabatic effect induces a change of the polymer rheology. Consequently, a drop of AE events and AE energy occurs due to plastic shearing source of less energetic AE. At longer term, as the cumulated number of hits keeps increasing, even when a great contact conformity is reached, the two interfacial mechanisms remain active. Indeed, over a sliding distance of 3 m, the contact also keeps slightly evolving regarding the average friction $\langle\mu\rangle$. In particular, when the contact is unidirectional, the sliding is never supported by the polymer relaxation which favors large plastic deformations and stretches ridges formation along the sliding direction. In this case, the AE signals is represented by more events at the frequency around 1 MHz than in reciprocating sliding.

7. Conclusion

The wear mechanisms in a steel/PEKK sliding contact were studied in correlation to the acoustic emission (AE). Before the tribological experiments the semicrystalline PEKK polymer was characterized by DSC showing a glass transition around 150 °C and a melting temperature around 300 °C. The DMTA analysis also displayed the drop of mechanical properties after the glass transition. The stress relaxation tests showed that the first time of the polymer relaxation is around 8 s. These properties were put in correlation to the tribological behavior of the PEKK which highlights the following conclusions:

- During the reciprocal sliding tests, the friction displays a periodic form with a high phase of friction HF and a low phase of friction LF. Actually, during the HF phase, the slider push in compression the polymer and during the forward motion, corresponding to the LF phase, the viscoelastic recovery assist the motion. Inversely, the amplitude of AE is higher during the LF phase than during the HF phase.
- The friction coefficient decreases with the load accordingly to lower contribution of molecular attraction forces. The friction also decreases with the velocity and more broadly with the cumulated mechanical energy. This is due to an adiabatic effect in the contact which provokes a change of the polymer rheology.
- The Schallamarch ridges formation are resulting from nanometric interaction between asperities and represents a source of AE with a representative frequency around 1 MHz. The mechanism of ploughing generating microscopic longitudinal scratches is a source of AE with a lower frequency around 0.2 MHz.
- Reciprocal sliding and unidirectional sliding give different results of friction, wear and AE. During reciprocal sliding, the polymer relaxation greatly influences the polymer tribological behavior. The unidirectional sliding produces larger plastic deformation and stretched Schallamarch ridges in the direction of sliding. This change of mechanisms is visible on AE by the greater number of hits generated around the frequency of 1 MHz.

[1] J. Geringer, W. Tatkiewicz, G. Rouchouse, Wear behavior of PAEK, polu(aryl-ether-ketone), under physiological conditions, outlooks for performing these materials in the field of hip prosthesis, wear 271 (2011) 2793–2803.

[2] D. F. Moore, Principles and Applications of Tribology, Pergamon International Library, 1975, Ch. Friction of elastomers, pp. 61–85.

[3] M. Barquins, Adherence, friction and wear of rubber-like materials, wear 158 (1992) 87–117.

[4] K.L. Johnson,K. Kendall, A.D. Roberts, Surface energy and the contact of elastic solids, Proceedings of the Royal Society of London A: Mathematical, Physical and Engineering Sciences 324 (1971) 301–313.

[5] A. Schallamach, Abrasion pattern on rubber, Rubber Chemistry and Technology 26 (1953) 230–241.

[6] A. K. Bhowmick, Ridge formation during the abrasion of elastomers, Rubber Chemistry and Technology 55 (1982) 1055–1062.

[7] M. Yahiaoui, J. Denape, J.-Y. Paris, A.G. Ural, N. Alcalá, F.J. Martínez, Wear dynamics of a TPU/steel contact under reciprocal sliding, Wear 315 (2014) 103–114.

[8] S. Ramachandra, T. C. Ovaert, The effect of controlled surface topographical features on the unlubricated transfer and wear of PEEK, Wear 206 (1997) 94–99.

[9] Y. Berthier, Maurice godet's third body, in: The Third Body Concept Interpretation of Tribological Phenomena, Vol. 31 of Tribology Series, Elsevier, 1996, pp. 21 – 30.

[10] Z. P. Lu, K. Friedrich, On sliding friction and wear of PEEK and its composites, Wear 181-183 (1995) 624–631.

[11] V. Baranov, E. Kudryavtsev, G. Sarycgev, V. Schavelin. Acoustic emission in friction, Elsevier, 2007.

[12] M. Yahiaoui, J.-Y. Paris, J. Denape, Correlation between acoustic emission signals and friction behavior under different sliding configurations and materials pairs, Key Engineering Materials 640 (2015) 21–28.

[13] A. Hase, H. Mishina, M. Wada, Correlation between features of acoustic emission signals and mechanical wear mechanisms, Wear 292-293 (2012) 144–150.

[14] C. Ferrer, F. Salas, M. Pascual, Discrete acoustic emission waves during stick-slip friction between steel samples, Tribology International 43 (2010) 1–6.

[15] D.V. Lychagin, A.V. Filippov, O.S. Novitskaia, E.A. Kolubaev, O.V. Sizova, Experimental Research Into Generation of Acoustic Emission Signals in the Process of Friction of Hadfield Steel Single Crystals, IOP Conf. Series: Materials Science and Engineering 142 (2016) 012098.

[16] H. Taura, K. Nakayama, Behavior of acoustic emissions at the onset of sliding friction, Tribology International 123 (2019) 155–160.

[17] S. Dolinšek, J. Kopač, Acoustic emission signals for tool wear identification, Wear 225–229 (1999) 295–303.

[18] A. Hase, M. Wada, H. Mishina, Scanning electron microscope observation study for identification of wear mechanism using acoustic emission technique, Tribology International 72 (2014) 51–57.

[19] D.W. Cherry, Polymer surface, Cambridge University Press, 1981.

[20] M. Barquins, Friction and wear of rubber-like materials, Wear 160 (1993) 1–11.

[21] D. Tabor. Friction, Adhesion and Boundary Lubrication of Polymers, Springer, 1974.

[22] K. Tanaka, Y. Uchiyama, Friction, Wear and Surface Melting of Crystalline Polymers, Advances in Polymer Friction and Wear, Polymer Science and Technology, 1974.

[23] B.J. Briscoe, S.K. Sinha, Tribology of Polymeric Solids and Their Composites, in: Wear: Materials, mechanisms & practice, 2005

[24] Heat capacities of high melting polymers containing phenylene groups, Polymer, 28 (1087) 10–22.